

We are IntechOpen, the world's leading publisher of Open Access books Built by scientists, for scientists

4,800

Open access books available

122,000

International authors and editors

135M

Downloads

Our authors are among the

154

Countries delivered to

TOP 1%

most cited scientists

12.2%

Contributors from top 500 universities

**WEB OF SCIENCE™**Selection of our books indexed in the Book Citation Index
in Web of Science™ Core Collection (BKCI)

Interested in publishing with us?
Contact book.department@intechopen.com

Numbers displayed above are based on latest data collected.

For more information visit www.intechopen.com

Modelling of Precipitation Hardening in Casting Aluminium Alloys

Linda Wu and W. George Ferguson
*University of Auckland
New Zealand*

1. Introduction

Precipitation hardening, because it involves the hardening of the material over a prolonged time, is also called age hardening, or ageing. By the appropriate heat treatment of precipitation hardening, the strength or hardness of some heat-treatable aluminium alloys can be enhanced by the formation of nano-meter sized second-phase precipitated particles within the original phase matrix. The fine precipitates in the alloy impede dislocation movement by forcing the dislocations to either cut through the precipitated particles or go around them. By restricting dislocation movement during deformation, the alloy is strengthened. Thus precipitation hardening is the most versatile and demanding heat treatment in aluminium alloys, either for wrought or casting alloys.

The precipitation-hardening process generally involves following three basic steps:

- a. Solution heat treatment, or homogenization, is the first step where the alloy is heated between the solvus and solidus temperatures and soaked until all of the soluble phases are dissolved and a homogeneous solid-solution structure is produced.
- b. Quenching is the second step where the solid solution is rapidly cooled to a lower temperature, usually room temperature. This forms the formulation of a supersaturated solid solution (SSSS) since the solubility of one or more alloying elements in aluminium decreases with decreasing temperature.
- c. The final step in the precipitation hardening process is aging that allows controlled decomposition of the supersaturated solid solution (SSSS) and the formation of strengthening precipitates. It is the process where the supersaturated solution is heated below the solvus temperature to produce a finely dispersed precipitates. When ageing occurs at room temperature, it is called natural ageing. Ageing above room temperature is called artificial ageing.

With the age-hardening aluminium alloys having become the backbone of the automotive and aerospace industries, although a century has now elapsed since the phenomenon of age or precipitation hardening was discovered by the German metallurgist, Alfred Wilm (Wilm, 1911), new observations are still being made as the latest experimental techniques reveal more details of the actual atomic process involved. Precipitation hardening was hailed as the first nanotechnology (Polmear, 2006) and now it is possible to develop fine-scale microstructures in a much wider range of alloys through the use of novel processing methods. The optimization of material processing techniques has, however, for a long time,

been pursued by trial and error. As it involves working blind, this method is costly and wasteful of manpower. It is desirable for material scientists to conduct fewer experiments to attain a specified goal. Fortunately, this has become possible with the development of materials and computer science.

Since the precipitation of second phase particles is critical to the properties of many industrially important aluminium alloys, modelling of precipitation kinetics and strengthening in age hardening aluminium alloys has gained considerable interest among researchers. During the precipitation process, three major physical elementary mechanisms are involved: i.e. nucleation, growth and coarsening. Based on how these three processes are treated, modelling of the precipitation kinetics in aluminium alloys can be divided into two main approaches. One of approaches is based on the Shercliff-Ashby process model (Shercliff & Ashby, 1990a) in which only one average particle size is assumed and the three processes are considered in isolation with the implicit assumption that one process is essentially complete before the next one begins. Shercliff and Ashby first attempted to assemble a process model for the ageing of the simplest of the age-hardening aluminium alloys, by introducing a process model widely used in chemical engineering but relatively rare in processing of solid materials. Their process model draws together established knowledge of the kinetics of microstructure evolution with dislocation behavior, in order to determine the mechanical properties. This model gives a good description of some Al-Cu and Al-Mg-Si (Shercliff & Ashby, 1990b), wrought as well as casting alloys (Rometsch & Schaffer, 2002) and also 8000 Al-Li aluminium alloys (Pandey, 1995).

In the other approach, which is more refined, Kampmann and Wagner have produced a numerical approach (KWN model) (Kampmann et al., 1987; Kampmann & Wagner, 1984) capable of describing the particle size distribution (PSD) in the time domain, while dealing with the nucleation-growth-coarsening phenomena within the same formulation. Hence in the KWN model, the particle size is assumed to be a continuous parameter. And then a strength model is used to evaluate the resulting change in hardness or yield strength at room temperature by taking into account contributions from lattice resistance, solid solution hardening and precipitation hardening. Though the KWN model has been developed for a few decades and successfully applied to a number of aluminium alloy systems, such as 2xxx, 6xxx and 7xxx (Myhr & Grong, 2000; Myhr *et al.*, 2001; Robson, 2004a; Robson, 2004b), however, most of modelling work has been focused on the wrought aluminium alloys and none modelling work has been applied to the casting aluminium alloys. In the present work, the KWN model has been for the first time applied to the casting aluminium alloys A356 and A357.

2. Shercliff-Ashby process model

2.1 Components of the process model

The complete Shercliff-Ashby model for isothermal age hardening includes the following components or – best called sub-models:

1. The initial growth of a volume fraction of precipitate, and consequent changes in solute concentration;
2. The dependence of the equilibrium volume fraction of precipitate on ageing temperature;
3. Precipitate coarsening by competitive growth;
4. The contribution of solid solution strengthening to the yield strength;

5. The contribution of shearable precipitates to the strength; and
6. The contribution of non-shearable or bypassing precipitates to the strength (Orowan Strengthening).

The sub-models (1) ~ (3) belong to the microstructure evolution. And the contributions to the strength model consist of the sub-models (4) ~ (6).

2.1.1 Precipitation from supersaturated solid solution

After solution heat treatment and quenching, the non-equilibrium phase precipitates from the solid solution on ageing. During the early stages of precipitation, the initial precipitation kinetics are described by Shewmon (Shewmon, 1963): the mean solute concentration in the matrix \bar{c} decays exponentially with time t , raised to a power close to unity:

$$\bar{c}(t) = c_e + (c_i - c_e) \exp(-t / \tau_1) \quad (1)$$

where c_i is the initial solute concentration, c_e is the solute concentration at equilibrium at the ageing temperature, and τ_1 is a temperature-dependent time constant.

The volume fraction f of precipitate is directly proportional to solute loss $c_i - \bar{c}(t)$, tending to a final equilibrium value, f_e , when $\bar{c} = c_e$, thus:

$$\frac{f(t)}{f_e} = \frac{c_i - \bar{c}(t)}{c_i - c_e} = 1 - \exp(-t / \tau_1) \quad (2)$$

2.1.2 The dependence of f_e on ageing temperature

The concentration of solute at the metastable solvus temperature c_s is described by (Swalin, 1962):

$$c_s = A_0 \exp(-Q_s / RT_s) \quad (3)$$

Where A_0 is a constant, and Q_s is the free energy of solution of the solute, T_s is solid solvus temperature.

The equilibrium concentration of solute c_e at a temperature $T < T_s$ is:

$$c_e = A_0 \exp(-Q_s / RT) \quad (4)$$

Dividing the above two equations gives the following equation:

$$c_e = c_s \exp \left[-Q_s \left(\frac{1}{T} - \frac{1}{T_s} \right) \right] \quad (5)$$

The equilibrium volume fraction of precipitate at temperature T is given by:

$$f_e = f_{\max} \left(\frac{c_s - c_e}{c_s} \right) \quad (6)$$

where f_{\max} is the maximum possible volume fraction precipitated at absolute zero. Substituting from equation (5):

$$f_e = f_{\max} \left\{ 1 - \exp \left[-\frac{Q_s}{R} \left(\frac{1}{T} - \frac{1}{T_s} \right) \right] \right\} \quad (7)$$

The above equation shows the dependence of f_e on how far the ageing temperature T lies below the (metastable) solid solvus temperature, T_s .

2.1.3 Particle coarsening

Since the coarsening of precipitates was first described by Ostwald (Ostwald, 1900), particle coarsening is often called Ostwald ripening. Most theories of Ostwald ripening are based on the classical works of Lifshitz and Slyozov (LS) (Lifshitz & Slyozov, 1961) and of Wagner (Wagner, 1961), commonly referred to as LSW theory. The LSW theory predicts a cube law relating the mean particle radius \bar{r} at time t to that, \bar{r}_0 , at time $t = 0$:

$$\bar{r}^3(t) - \bar{r}_0^3 = \frac{c_1 t}{T} \exp\left(-\frac{Q_A}{RT}\right) \quad (8)$$

Where c_1 is a constant, Q_A is the activation energy for volume diffusion of atoms between particles, R the Universal gas constant (8.314 J/mol K) and T the aging temperature.

2.1.4 The contribution of the solid solution to the strength $\Delta\sigma_{ss}$

For this strengthening mechanism, solute atoms of one element are added to another, resulting in either substitutional or interstitial point defects in the crystal. The substitution of solute atoms for aluminium atoms distorts the crystal lattice, hinders dislocation mobility and hence strengthens the alloy. The glide resistance caused by a solute at a mean concentration \bar{c} , expressed as a contribution to the yield strength, $\Delta\sigma_{ss}$, is given by (Friedel, 1964; Nabarro, 1967; Cottrell, 1964; Nabarro *et al.*, 1979; Hospital, 1987; Hull & Bacon, 2001):

$$\Delta\sigma_{ss} = c_2 [\bar{c}_j]^{2/3} \quad (9)$$

where c_2 is a constant related to the size, modulus and electronic mismatch of the solute including various resolution factors, and \bar{c}_j , the mean solute concentration of a specific alloying element in the matrix.

2.1.5 The contribution of shearable precipitates to the strength $\Delta\sigma_A$

When particles are small, the dislocations will shear the precipitates, which is sometimes called precipitate resistance (Cahn *et al.*, 1996). For this cutting mechanism, the contribution of shearable precipitates to the yield strength can be represented by:

$$\Delta\sigma_A = c_3 f^m \bar{r}^n = c_3 f^{1/2} \bar{r}^{1/2} \quad (10)$$

where c_3 is an alloy constant that depends on the particular strengthening mechanism, i.e., coherency, surface, chemical, stacking fault, and/or modulus hardening. The exponents m and n are always positive, for most dislocation particle interactions, both m and n have the values 0.5 (Starke, 1977; Sanders, 1980).

2.1.6 The contribution of bypassing precipitates to the strength $\Delta\sigma_B$

When the precipitates grow during the precipitation the strength is increased and the dislocation can no longer cut the precipitates. The mechanism by which dislocations bypass precipitates was first proposed by Orowan (Orowan, 1948) and is referred to as the Orowan mechanism or dispersed particle strengthening. A simple (but adequate) form of the Orowan equation is:

$$\Delta\sigma_B = \frac{c'Gb}{l} \quad (11)$$

where c' is a constant, G the shear modulus, and b the Burgers vector. The particle spacing, l , in the slip plane of the dislocation is related to the volume fraction, f , and radius, r . Substituting $l = c'' \frac{r}{f^{1/2}}$ (where c'' is a constant) into equation (11) gives:

$$\Delta\sigma_B = c_4 \frac{f^{1/2}}{r} \quad (12)$$

where c_4 contains all the constants in equations (11) and c'' .

2.2 Assembly of the process model

In real alloys where a number of different strengthening mechanisms are operative at room temperature (Hatch et al., 1984), it is reasonable to assume that the individual strength contributions can be added linearly. Considering age hardening aluminium alloys, the following contributions are of importance, i.e., with precipitation hardening due to shearing and bypassing of particles by dislocations and solid solution hardening effects. Therefore, the resulting expression for the overall macroscopic yield strength σ is:

$$\sigma = \sigma_i + \sigma_{ss} + \sigma_{ppt} \quad (13)$$

Where σ_i is the intrinsic yield strength, which remains constant during ageing. σ_{ss} is the solid solution strength and σ_{ppt} is the precipitation hardening strength due to shearing and bypassing of particles by dislocations.

The method of assembling the process model is to combine the microstructure evolution of sub-models into the different contributions to the yield strength (Kocks et al., 1975; Martin, 1980), then identify the overall yield strength with the sum. Both mean solute concentration \bar{c} and volume fraction f vary with time, reaching steady values before the peak of the ageing curve is reached.

In order to combine the equations of sub-models together to give a process model for ageing, Shercliff and Ashby proposed the *temperature corrected time*, P , which was defined by:

$$P = \frac{t}{T} \exp - \frac{Q_A}{RT} \quad (14)$$

This parameter, referred to as "kinetic strength" by Ion et al. (Ion et al., 1984), measures the number of kinetic jumps that have taken place in time t . Over most of the ageing curve, the initial radius $r_0 \ll r$, hence we may re-write equation (8):

$$r(t) = C_1 P^{1/3} \quad (15)$$

In the Shercliff-Ashby modeling work, the net contribution of precipitation to the strength from the shearing and bypassing precipitates was defined by taking their harmonic mean:

$$\Delta\sigma_{ppt} = \left[\frac{1}{\Delta\sigma_A} + \frac{1}{\Delta\sigma_B} \right]^{-1} \quad (16)$$

If define the value of P corresponding to the peak strength as P_p and the volume fraction f reaches an equilibrium volume fraction f_e , then from the fact that the peak in the ageing curve lies very close to the point where the two contributions to peak strengthening are equal, $\Delta\sigma_A = \Delta\sigma_B$, and we can get $C_3 f_e^{1/2} P P^{1/6} = C_4 f_e^{1/2} P_p^{-1/3}$, which gives the relationship:

$$C_4 = C_3 P_p^{1/2} \quad (17)$$

From the equation (17), we can conclude that the value of P required to reach the peak over a wide range of temperature is often roughly constant. Its value can be found from equation (14) by substituting values for the times t_p corresponding to the peaks of the ageing curves at several temperatures and taking the mean. Hence we use this value, P_p , to normalize the kinetic strength (noting that $P/P_p = 1$ at the peak), equation (15) becomes:

$$r(t) = C_5 \left(\frac{P}{P_p} \right)^{1/3} \quad (18)$$

Then another parameter S_0 , the "peak precipitation strength" is introduced into the model and defined by:

$$S_0 = \frac{C_3}{2} f_e^{1/2} P_p^{1/2} \quad (19)$$

Because P_p is constant, $S_0^2 \propto f_e$. Substituting r and S_0 into equations (10) and (12) and then taking the harmonic mean gives:

$$\Delta\sigma_{ppt} = \frac{2S_0 \left(P/P_p \right)^{1/6}}{1 + \left(P/P_p \right)^{1/2}} \quad (20)$$

Note that when $P = P_p$, $\Delta\sigma_p = S_0$, which defines the peak in the ageing curve.

Since $S_0^2 \propto f_e$ and according to equation $f(t) = f_e * [1 - \exp(-t/\tau_1)]$, by assuming the cubic coarsening law holds from the very beginning of precipitation even while the volume fraction is changing, and replacing f_e by $f(t)$, gives a corresponding variation in S^2 :

$$S^2(t) = S_0^2 [1 - \exp(-t/\tau_1)] \quad (21)$$

From these equations it may deduced that when $t \gg \tau_1$, $f(t)$ tends to f_e and $S(t)$ has reached the peak precipitate strength, S_0 .

From equation (9), the initial solute concentration c_i can be expressed in terms of the initial solid solution strength $\Delta\sigma_{ssi}$, that is, $c_i = c_4\Delta\sigma_{ssi}^{3/2}$; and similar equilibrium solute concentration c_e can be expressed in terms of the final solid solution strength contribution $\Delta\sigma_{ss0}$, that is, $c_e = c_4\Delta\sigma_{ss0}^{3/2}$. Substituting these expressions into equation (1) gives:

$$\bar{c}(t) = c_4[\Delta\sigma_{ss0}^{3/2} + (\Delta\sigma_{ssi}^{3/2} - \Delta\sigma_{ss0}^{3/2}) \times \exp(-t / \tau_1)] \quad (22)$$

Substituting this value into equation (9), the evolution of the corresponding solid solution strength is then described by:

$$\Delta\sigma_{ss}(t) = \left[\Delta\sigma_{ss0}^{3/2} + (\Delta\sigma_{ssi}^{3/2} - \Delta\sigma_{ss0}^{3/2}) \times \exp(-t / \tau_1) \right]^{2/3} \quad (23)$$

Experiments have shown that the volume fraction and solute concentration reach their equilibrium values at a time which is a constant fraction of the time to reach peak strength (Anderson, 1959). Therefore, the time constant τ_1 in the equations can be scaled as t_p :

$$\tau_1 = K_1 t_p \quad (24)$$

where K_1 is a constant.

Or using the definition of P_p :

$$\tau_1 = K_1 P_p T \exp(Q_A / RT) \quad (25)$$

The peak precipitate strength S_0 depends on the ageing temperature because the volume fraction f_e does so. Combining this with equation (21) gives:

$$S_0^2(T) = (S_0)_{\max}^2 \left\{ 1 - \exp \left[-\frac{Q_s}{R} \left(\frac{1}{T} - \frac{1}{T_s} \right) \right] \right\} \quad (26)$$

Combining equation (7) and (26) gives:

$$S^2(t, T) = (S_0)_{\max}^2 \left\{ 1 - \exp \left[-\frac{Q_s}{R} \left(\frac{1}{T} - \frac{1}{T_s} \right) \right] \right\} \times [1 - \exp(-t / \tau_1)] \quad (27)$$

Similarly the solid solution contribution to the strength depends on the ageing temperature because it determines the amount of solute left in solution. The temperature-variation of the equilibrium solid solution component of the yield strength is:

$$\begin{aligned} (\Delta\sigma_{ss0})_T &= c_2(c_e)^{2/3} \\ &= (\Delta\sigma_{ss0})_{T_s} \exp \left[-\frac{2}{3} \frac{Q_s}{R} \left(\frac{1}{T} - \frac{1}{T_s} \right) \right] \end{aligned} \quad (28)$$

At $T = T_s$, the concentration of the matrix equals the alloy concentration, and there is no precipitate. In the as-quenched condition the alloy is a uniform solution of the full alloy content, hence the as-quenched strength, σ_q , is given by:

$$\sigma_q = \sigma_i + (\Delta\sigma_{ss0})_{T_s} \quad (29)$$

By combining equation (28) and (29) gives:

$$(\Delta\sigma_{ss0})_T = (\sigma_q - \sigma_i) \exp\left[-\frac{2}{3} \frac{Q_s}{R} \left(\frac{1}{T} - \frac{1}{T_s}\right)\right] \quad (30)$$

In the over-aged condition, the coarse precipitate contribute to the strength can be negligible, hence the over-aged strength σ_{oa} depends only on the matrix solute concentration. Thus σ_{oa} is the sum of the solid solution strength and the intrinsic strength of pure aluminium σ_i :

$$(\sigma_{oa})_T = \sigma_i + (\Delta\sigma_{ss0})_T \quad (31)$$

Combining equations (30) and (31) gives the variation of the over-aged strength with temperature:

$$(\Delta\sigma_{oa})_T = \sigma_i + (\sigma_q - \sigma_i) \exp\left[-\frac{2}{3} \frac{Q_s}{R} \left(\frac{1}{T} - \frac{1}{T_s}\right)\right] \quad (32)$$

Using known values of σ_i and σ_q , the over-aged strength can be calculated.

2.3 Calibration of the model

The most difficult aspect in application of the Shercliff-Ashby model is calibration of the constants used in the process model. There are six constants that need to be calibrated from ageing curves: activation energy for ageing Q_A (KJ mol⁻¹), peak temperature-corrected time P_p (s K⁻¹), metastable solvus temperature T_s (°C), solvus enthalpy Q_s (KJ mol⁻¹), maximum strength parameter at absolute zero $(S_0)_{\max}$ (MPa), constant coefficient K_1 relating τ_1 to t_p . These constants do not change with temperature for the specific alloy.

2.3.1 Calibration Q_A and P_p

Q_A and P_p can be found by calibrating the data to the peaks of the ageing curves. The values of peak hardness σ_p and the time to peak t_p at various temperatures can be read from the ageing curves. By finding the time to peak t_p at various temperatures, P_p is evaluated directly.

From equation (14) it can be deduced that $P_p = \frac{t_p}{T} \exp\left(\frac{-Q_A}{RT}\right) = \text{constant}$, and taking natural logs it becomes:

$$\ln P_p = \ln(t_p / T) - (Q_A / RT) \quad (33)$$

By putting $x = 1/T$ and $y = \ln(t_p / T)$, an Arrhenius plot of y against x results in a straight line. The value of Q_A can be derived from the slope (Q_A / R). The value of P_p can be either calculated from $y_0 = \ln P_p$ when $x = 0$, or taken as the mean value of P_p at each temperature.

2.3.2 Calibration $(S_0)_{\max}$, Q_s and T_s

The temperature dependence of the equilibrium volume fraction is contained in the parameter S_0 since $S_0^2 \propto f_e$. From equation (26), by plotting S_0^2 against temperature enables

us to find values for $(S_0)_{\max}$ and T_s . From the graph, at the intersection of the extrapolated curve with the temperature axis, $S_0^2 = 0$, and from equation (26), it can be deduced that $T = T_s$; at the intersection with the S_0^2 axis, $T = 0$, it can be deduced that $S_0 = (S_0)_{\max}$. When $(S_0)_{\max}$ and T_s have been determined, the solvus enthalpy Q_s for each ageing temperature can be calculated using:

$$Q_s = \frac{-R}{(1/T - 1/T_s)} \ln \left[1 - \frac{S_0^2}{(S_0)_{\max}^2} \right] \quad (34)$$

The main problem is how to determine the value of S_0 from the ageing curves. At peak ageing, $(\Delta\sigma_{ppt})_p = S_0$. The peak precipitation strength contribution, $(\Delta\sigma_{ppt})_p$, is found by subtracting the other contributions (solid solution $\Delta\sigma_{ss}$ and intrinsic σ_i) from the measured peak strength σ_p .

$$(\Delta\sigma_{ppt})_p = S_0 = \sigma_p - (\Delta\sigma_{ss} + \sigma_i) \quad (35)$$

At peak hardness, the other contribution to $(\Delta\sigma_{ss} + \sigma_i)$ is the over-aged strength σ_{oa} since f has reached its equilibrium value f_e before the peak. The value of σ_{oa} , however, depends on the value of Q_s and T_s as described by equation (32), which are not known. Thus we have to use an iterative method. We first estimate the value of σ_{oa} : it must lie between the as quenched strength σ_q (when all the solute is in solution), and the intrinsic strength σ_i (when no solute is left in solution). Thus:

$$(\sigma_{oa})_{est} = (\Delta\sigma_{ss0} + \sigma_i)_p = (\sigma_i + \sigma_q) / 2 \quad (36)$$

Thus, using equation (36) an initial estimated value of S_0 is obtained by:

$$(S_0)_{est} = \sigma_p - (\sigma_{oa})_{est} \quad (37)$$

For each ageing temperature, it is possible to get the value of $(S_0)_{est}$. A graph of $(S_0)_{est}^2$ against temperature T is then plotted. From the graph, the first estimated values of $(S_0)_{\max}$ and T_s are obtained and Q_s is calculated from equation (34).

From these values of Q_s and T_s , a better estimate of σ_{oa} and S_0 may now be obtained using equations (36) and (37). The whole procedure is repeated until the fit between theory and data is satisfactory.

2.3.3 Calibration of K_1

It remains to determine the time constant τ_1 which is related to the peak temperature corrected time by equation (25). The constant K_1 is adjusted to give the required decay. The decay of the solid solution component of the strength is then given by equation (23) with $\Delta\sigma_{ssi} = \sigma_q - \sigma_i$ and $\Delta\sigma_{ss0} = \sigma_{oa} - \sigma_i$.

2.4 Application of the model

The modelling method is applied to casting alloys A356 and A357. All the processes for calibration and constructing the predicted ageing curves are programmed under MATLAB

which is a large software package that has many advanced features built-in, and it has become a standard tool for many working in science or engineering disciplines.

2.4.1 Input data

The input data for each alloy includes its composition, as quenched strength σ_q and the strength of σ_i , which is defined as being the sum of the intrinsic strength of pure aluminium and solid solution strengthening contributions which remain constant during ageing, as well as the information of ageing curves which includes temperature T , time to peak yield strength t_p and the peak yield strength σ_p . All this information is used to calibrate the constants thus the predicted ageing curves for various temperatures can be constructed.

The most detailed data set available was from Rometsch, etc. (Rometsch & Schaffer, 2002) for the ageing of casting alloy A356 & A357 at various temperatures. The compositions (in wt.%) are to be Al-7.0 Si-0.40Mg-0.13Fe-0.03Sr for A356 and Al-7.0 Si-0.60Mg-0.13Fe-0.03Sr for A357. The equilibrium precipitates are Mg_2Si . σ_i is 43 MPa and as quenched strength $\sigma_q = 75$ MPa for A356 and $\sigma_q = 85$ MPa for A357. All above data with a data set for peak time and yield strength at various temperatures are listed in Table 1 & Table 2.

Nominal composition of Mg (wt%)	1.0		
σ_i (MPa)	43		
σ_q (MPa)	75		
Ageing data	Temperature T (°C)	Time to peak t_p (s)	Peak YS σ_p (MPa)
	250	268	207
	230	699	239
	210	1630	256
	190	5188	271
	170	39,156	268
	150	263,090	272

Table 1. Data used for calibration for A356

Nominal composition of Mg (wt%)	1.0		
σ_i (MPa)	43		
σ_q (MPa)	85		
Ageing data	Temperature T (°C)	Time to peak t_p (s)	Peak YS σ_p (MPa)
	250	191	258
	230	503	277
	210	979	294
	190	4354	297
	170	34,026	300
	150	267,881	303

Table 2. Data used for calibration for A357

2.4.2 Calibration results

The calibration results for the alloys A356 and A357 using the above input data are listed in Table 3.

Parameter	Symbol	A356	A357
Activation energy for ageing (KJ mol ⁻¹)	Q_A	130.38	137.66
Peak temperature-corrected time (s K ⁻¹)	P_p	3.58×10^{-14}	4.36×10^{-15}
Metastable solvus temperature (°C)	T_s	269.59	286.66
Solvus enthalpy (kJ mol ⁻¹)	Q_s	55.39	50.30
Maximum strength parameter at absolute zero (MPa)	$(S_0)_{\max}$	229.70	259.34
Constant relating τ_1 to t_p	K_1	0.0990	0.1009

Table 3. Calibration results for A356, A357

2.4.3 Modelling results

The contributions to the full ageing curve of the intrinsic strength, solid solution strength, and precipitation hardening due to shearable and non-shearable stresses for A356 at 175 °C are shown in Fig.1. The net contribution of precipitation to the strength from the shearing and bypassing precipitates was modelled by taking their harmonic mean.

After calibration, the ageing curves for different isothermal ageing temperatures for alloys A356 and A357 were modelled, as shown in Fig. 2 and Fig. 3 respectively. And the values of t_p and σ_p for the different Al-Mg-Si alloys are listed in Table 4.

Material		Ageing at 50°C	Ageing at 100°C	Ageing at 150°C	Ageing at 175°C	Ageing at 190°C	Ageing at 210°C
A356	t_p (hour)	10000*	2400	20.00	2.75	0.93	0.24
	σ_p (MPa)	100.26*	284.60	282.97	279.79	275.95	266.62
A357	t_p (hour)	10000*	3000	19.00	2.33	0.74	0.18
	σ_p (MPa)	104.22*	316.21	314.70	312.01	308.92	301.78

t_p is limited to 100000 hours, * means not to peak ageing yet.

Table 4. t_p and σ_p for ageing at different temperatures for A356, A357

From Fig. 2 and Fig. 3 and Table 4, we can see that:

- The modelling results show that when ageing at a lower temperature, it takes a longer time to reach peak yield strength (or hardness), but the peak yield strength is higher, and vice versa. This is the basic ageing trend.

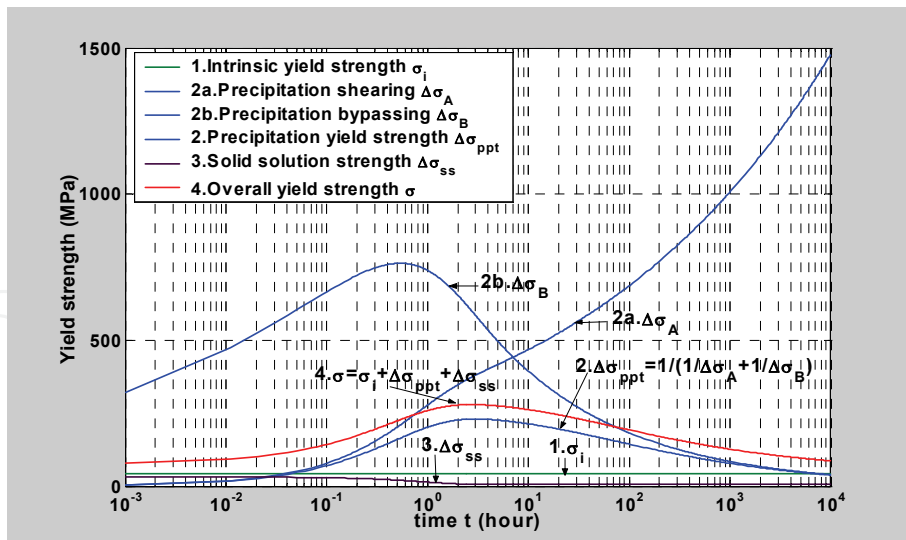


Fig. 1. Ageing curve of different contributions for A356 ageing at 175°C

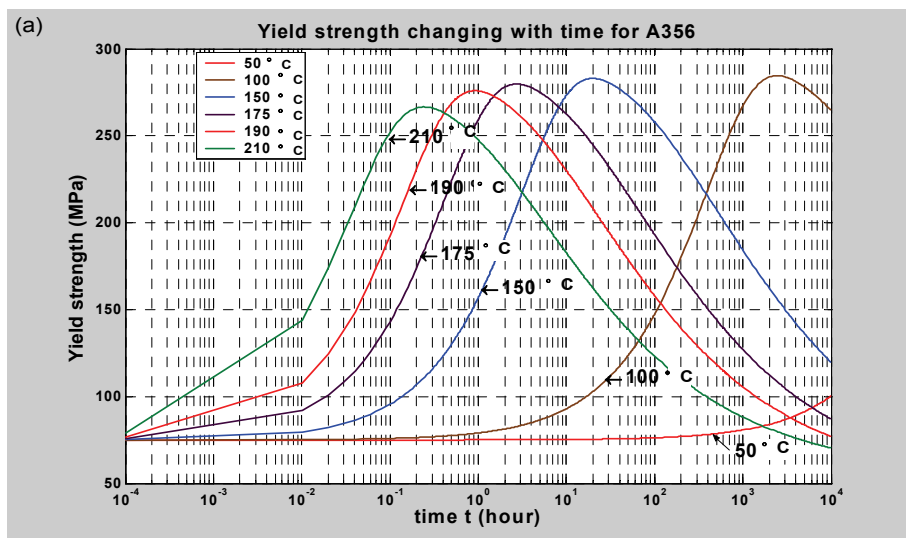


Fig. 2. Ageing at different temperatures for A356

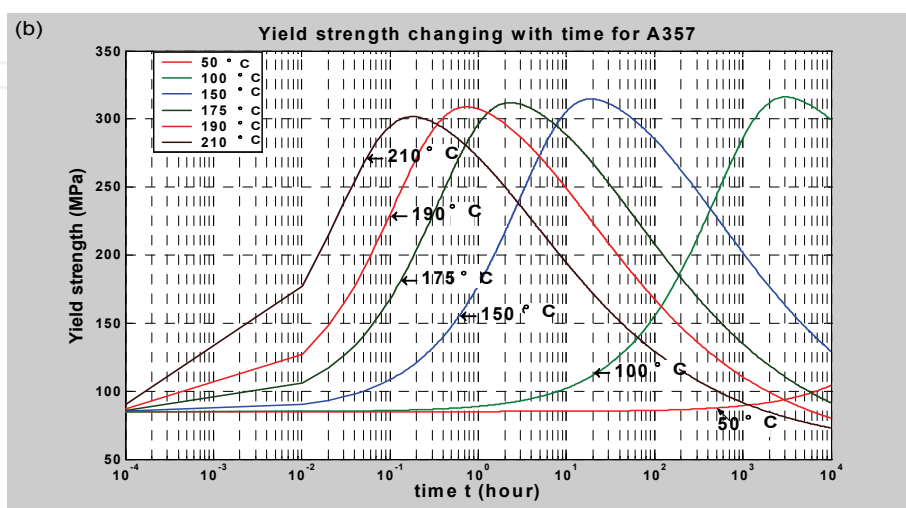


Fig. 3. Ageing at different temperatures for A357

- b. Time to the peak yield strength t_p is very sensitive to the temperature; however, the peak yield strength σ_p doesn't change much as temperature changes.
- c. At low temperature (such as 50°C), there is almost no yield strength or hardness gain for the initial of which means that the modeling results shows poor agreement with the experimental data at low temperatures.

2.4.4 Model validation

The modelling results are validated by ageing A356 at different temperatures, and recording hardness at different ageing times. The samples were cut from as cast A356 aluminium wheels, ground flat and the testing surfaces were finished with 1200 grit SiC paper.

The samples were solution treated in an unstirred salt bath at 540 ± 3 °C for 75 minutes, then quenched in water to room temperature and aged without delay. Artificial ageing was carried out in an oil bath (for 150°C) and salt baths (for 175°C, 210°C) with a temperature variation of ± 2 °C. At various times, a sample was removed from the bath then quenched in water to room temperature, and Rockwell hardness tests for Scale E and Scale K were done. For long ageing processes the samples were transferred to an air furnace after initial ageing in an oil or salt bath. Following heat treatment and before hardness testing, the artificial ageing samples were kept in a refrigerator, and natural ageing samples were kept at room temperature. The average value of at least five effective readings were used for each data point. The ageing curves for hardness are shown in Fig. 4.

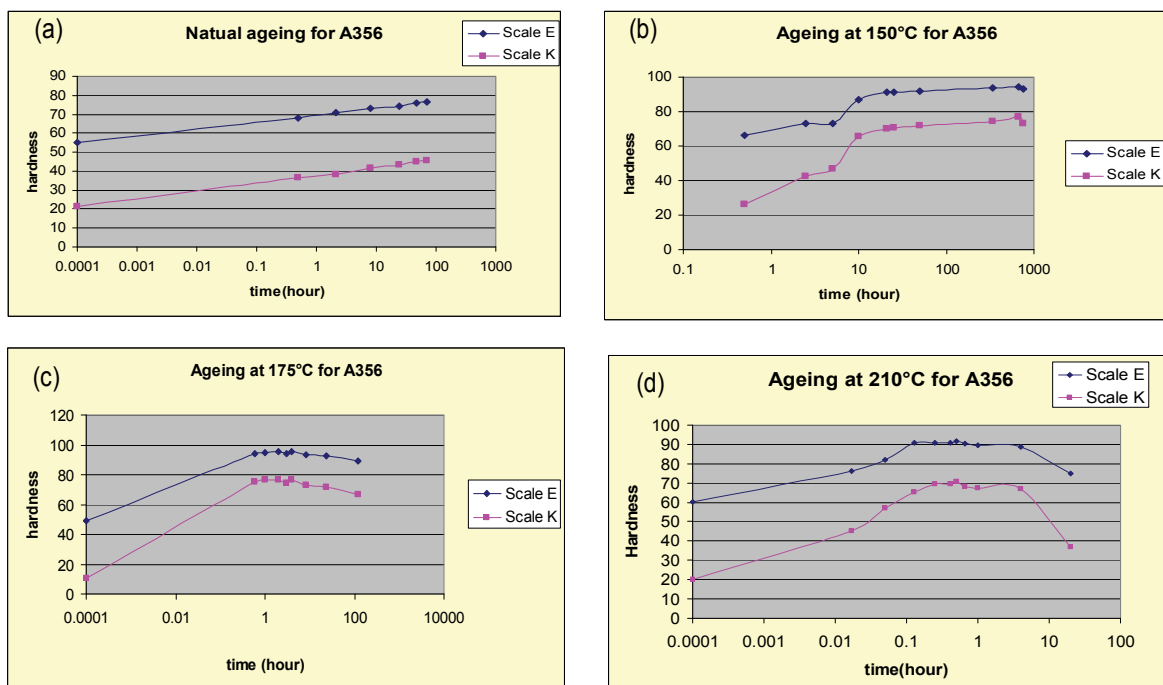


Fig. 4. Hardness changes with time for A356 at (a) Natural ageing; (b) 150°C; (c) 175°C; (d) 210°C

From the above ageing curves, we can see that the experimental data is in good agreement with the modelling results for artificial ageing. However, for natural ageing, the hardness (or yield strength) increases with time, whereas the modeling curve shows almost no change for the initial 100 hours. This means that at lower temperature, the modeling results for Schercliff-Ashby method were in poor agreement with the experimental data. This could be

due to two reasons: the first is that among the input data used for calibration there is no information for low temperatures; the other reason is that in the present model, the ageing curve is mainly controlled by particle coarsening, with negligible input from nucleation and growth. Because for low temperature, it may take a longer time to reach the process of particle coarsening, nucleation and growth can not be neglected. Therefore, for the present calibration of the Schercliff–Ashby modelling method it is recommended that it not be applied at low ageing temperature.

3. Kampmann and Wagner Numerical model (KWN model)

The KWN model consists of the following two distinct but integrated modules:

- a. A microstructure model for prediction of the precipitation kinetics during ageing with coupled nucleation, growth and coarsening (and likewise dissolution) in dilute alloy systems, assuming spherical particles with uniform thermodynamic properties.
- b. A strength model, which converts the relevant output parameters into an equivalent room temperature yield stress or hardness.

3.1 Precipitation kinetics model

Modelling Microstructure evolution is the first step of any integrated model for predicting the properties of a given material. The modelling of precipitation kinetics is based on the Kampmann and Wagner type numerical model (KWN model). It has a number of features that make it suitable for industrial process modelling.

The essential features of this model are summarized below (Robson et al., 2003; Robson, 2008; Robson, 2004b):

- a. The continuous size distribution of the particles is subdivided into a large number of size classes $[R_j, R_{j+1}]$ containing N_j particles respectively.
- b. The continuous time evolution of the particle distribution is split up into a sequence of discrete time steps.
- c. At each time step, the number of newly nucleated particles with the size of slightly above the critical radius is calculated using classical nucleation theory and allocated to an appropriate size class.
- d. The growth of existing particles is calculated by assuming growth is diffusion controlled and spherical growth morphology. The influence of the Gibbs–Thomson effect is used to calculate the modified interfacial compositions for each size class at each time step. Therefore, the existing ones grow or shrink depending on their size.
- e. Coarsening arises naturally in the model, and no simplifying assumptions for the shape of the particle size distribution are pre-designed.
- f. The change in matrix solute level due to precipitate formation or dissolution is calculated at each time step using the mean field approximation.

3.1.1 Nucleation of new precipitates

According to classic nucleation theory, the nuclei form as a result of localised compositional fluctuations that occur statistically within the supersaturated matrix. Provided that the incubation period can be neglected at the same time as possible effects of elastic coherency strains around the nucleated particles are ignored, the nucleation rate j is conveniently expressed as (Myhr & Grong, 2000; Myhr et al., 1998; Myhr et al., 2004; Myhr et al., 2001; Myhr et al., 2002):

$$j = j_0 \exp \left[- \left(\frac{A_0}{RT} \right)^3 \left(\frac{1}{\ln(\bar{C}/C_e)} \right)^2 \right] \exp \left(- \frac{Q_d}{RT} \right) \quad (38)$$

where j_0 is a pre-exponential term, A_0 a parameter related to the potency of the heterogeneous nucleation sites in the parent material (J/mol), Q_d the activation energy for diffusion, \bar{C} the mean solute content in the matrix, and C_e is the equilibrium solute content at the particle/matrix interface (given by the phase diagram), R universal gas constant (8.314 J/Kmol), T temperature (K).

3.1.2 Particle growth

When a spherical particle of radius r and solute concentration C_p is embedded in a super-saturated solid solution of a mean concentration \bar{C} , it will either dissolve or grow, depending on whether the particle/matrix interface concentration C_i exceeds \bar{C} or not. According to the diffusion-controlled growth, under the mean field approximation, the growth rate of particles can be expressed as (Myhr & Grong, 2000; Myhr et al., 2001; Myhr et al., 2004; Wagner et al., 1991):

$$v = \frac{dr}{dt} = \frac{\bar{C} - C_i}{C_p - C_i} \frac{D}{r} \quad (39)$$

The diffusion coefficient D is calculated at a given temperature from:

$$D = D_0 \exp \left(\frac{-Q_d}{RT} \right) \quad (40)$$

The influence of interfaces on equilibrium (i.e. the interface curvature) has to be taken into account. This is the Gibbs-Thomson effect that modifies the solubility limits given by equilibrium thermodynamics (phase diagram). Through the Gibbs-Thomson equation (Madras & McCoy, 2003; Porter & Easterling, 1992; Miyazaki et al., 1996; Myhr et al., 2001):

$$C_i = C_e \exp \left(\frac{2\gamma V_m}{rRT} \right) \quad (41)$$

where γ is the particle-matrix interface energy, and V_m is the molar volume of the particle. Based on the above equations, it is possible to obtain an explicit expression for the critical radius r^* of a particle that neither will grow nor dissolve (Langer & Schwartz, 1980):

$$r^* = \frac{2\sigma V_m}{RT} \left(\ln \left(\frac{\bar{C}}{C_e} \right) \right)^{-1} \quad (42)$$

The radii of particles which nucleate in each time interval are tracked separately. As the fraction of solute in the matrix decreases during precipitation, the driving force for nucleation and growth of the precipitate particles decreases and the critical particle radius increases, reducing the nucleation rate with time. Because r^* depends on the current value of C_e , the thermal stability of the precipitates is sensitive to changes in the temperature during heat treatment. It follows that reheating promotes particle dissolution, whereas cooling or

isothermal annealing favours nucleation, growth and coarsening in a successive manner. Thus in the KWN model, the applied thermal programme has a large influence on the evolution of the particle size distribution with time.

3.1.3 Coarsening

Coarsening arises naturally in the model when the average solute concentration in the matrix \bar{C} becomes larger than the solute concentration at the precipitate/matrix interface C_i , thus resulting in the dissolution of the smaller precipitates. Therefore, those particles which have a radius $< r^*$ will have a negative growth rate according to equation (39) and will thus start to shrink. Particles with a radius $> r^*$ will retain a positive growth rate and will continue to increase in size. When the size of a group of particles reaches zero they are removed from the size distribution.

3.1.4 Mass balance

Once the volume fraction is computed, from the mass balance relating the amount of solute tied up in particles to the amount of the solute drained from the matrix, we can calculate the mean concentration in the matrix phase \bar{C} as:

$$\bar{C} = \frac{(C_0 - C_p f)}{(1 - f)} \quad (43)$$

where $f = \int_0^\infty \frac{4}{3}\pi r^3 \phi dr$ (ϕ is the size distribution function) is the volume fraction. The newly obtained matrix composition is employed as an input for the thermodynamic computations in the next time step.

3.2 Strength model

After predicting the microstructure evolution, the second step is to derive reliable microstructure/properties relationships. I will consider here the case of the yield stress or hardness. The strength model considering particle size distribution also includes precipitation hardening due to shearing and bypassing of particles by dislocations σ_p and solid solution hardening σ_{ss} .

3.2.1 Precipitation hardening

Pursuing the usual approach for determining the critical resolved shear stress (or yield strength) from the interaction of gliding dislocations with point obstacles (Ardell, 1985; Lloyd, 1985; Gerold, 1980), according to Deschamps and Brechet (Deschamps *et al.*, 1998; Deschamps & Brechet, 1998), the relationship between σ_{ppt} and \bar{F} is given as:

$$\sigma_{ppt} = \frac{M\bar{F}}{bL} \quad (44)$$

Where \bar{F} denotes the mean obstacle strength and σ_{ppt} the resulting increase in the overall macroscopic yield strength, M is the Taylor factor and b is the magnitude of the Burgers vector and L is the mean effective particle spacing in the slip plane along the curved dislocation. The microstructural variables \bar{F} and L evolve with aging time and are themselves functions of other microstructural variables as well as aging temperature.

Moreover, assuming a mono-dispersive system of spheres, the effective particle spacing L in the slip plane can be expressed in terms of the mean particle size \bar{r} , the particle volume fraction f , and the mean obstacle strength \bar{F} using the Friedel statistic (Friedel, 1964; Brown & Ham, 1971) which applies best for low obstacle strengths, and relies on the assumption of a steady-state for the number of precipitates along the dislocation line in motion. Thus, equation (44) becomes (Wagner et al., 1991; Deschamps & Brechet, 1998) :

$$\sigma_{ppt} = \frac{M}{b\bar{r}} (2\beta Gb^2)^{-1/2} \left(\frac{3f}{2\pi} \right)^{1/2} \bar{F}^{3/2} \quad (45)$$

where G is the shear modulus of the aluminium matrix and β is a constant close to 0.5. In the general case, where the alloy contains a mixture of weak (shearable) and strong (non-shearable) particles, the mean obstacle strength is conveniently defined as:

$$\bar{F} = \frac{\sum_i N_i F_i}{\sum_i N_i} \quad (46)$$

where N_i is the number density of particles that belongs to a given size class r_i , and F_i is the corresponding obstacle strength.

The obstacle strength depends on the mechanism of overcoming.

- In the case of particle shearing (weak particles), the obstacle strength can have a number of different dependencies on the particle radius, depending on the main interaction mechanism between the shearable particle and the dislocation. It is a fair approximation to assume that F_i is proportional to the particle radius as long as r is smaller than the critical radius for shearing r_c

$$\bar{F}_i = 2\beta Gb^2 \left(\frac{r_i}{r_c} \right) \quad (47)$$

- In the case of precipitate by-passing (strong particles, characterised by $r_i > r_c$), the obstacle strength is constant

$$\bar{F}_i = 2\beta Gb^2 \quad (48)$$

3.2.2 Solid solution hardening σ_{ss}

In age hardening, aluminium alloys elements, such as Mg, Si and Cu give rise to considerable solid solution strengthening. Provided that the contribution from each element is additive, the solid solution hardening potential of the alloy σ_{ss} can be expressed as:

$$\sigma_{ss} = \sum_j k_j C_j^{2/3} \quad (49)$$

where C_j is the concentration of a specific alloying element in solid solution and k_j is the corresponding scaling factor.

3.2.3 Overall yield strength and hardness

In alloys where several strengthening mechanisms are operative at room temperature, it is reasonable to assume that the individual strength contributions can be added linearly. Thus,

the resulting expression for the overall macroscopic yield strength σ is the same as the equation (13) used in Shercliff-Ashby model.

Conversion from yield strength (MPa) to hardness (VPN) can then be done through a simple regression formula (Grong, 1997):

$$H_v = 0.33\sigma_y + 16.0 \quad (50)$$

3.3 Application to the casting aluminium alloys

Although the KWN model has been successfully applied to different aluminium alloys (Myhr et al., 2001; Robson, 2004a), there are no reports of application to casting aluminium alloys. The present modelling work is the first time that KWN model has been applied to the casting aluminium alloys A356 and A357 for different ageing temperatures and compared with the experimental data.

3.3.1 Isothermal ageing

The modelling work is applied to the casting alloys A356 and A357 with chemical composition of Al-7.0Si-0.40Mg-0.13Fe-0.03Sr and Al-7.0Si-0.62Mg-0.13Fe-0.03Sr (Rometsch & Schaffer, 2002) by weight percentage respectively. The experimental data used to validate the model is obtained from the literature (Rometsch & Schaffer, 2002) and our experimental data. The yield strength is taken as approximately three times the Rockwell hardness scale E for A356.

The modelling results for ageing at various temperatures for A356 and A357 are shown in Fig. 5 and Fig. 6.

By choosing suitable parameters used in the microstructural and strength models, the modelled yield strength results for A356 (Fig. 5) and A357 (Fig. 6) are in very good agreement with the experimental data from the literature as well as own data. Because of greater Mg content, if ageing at the same temperature, the peak yield strength is higher and the time to peak ageing is shorter for A357 than for A356.

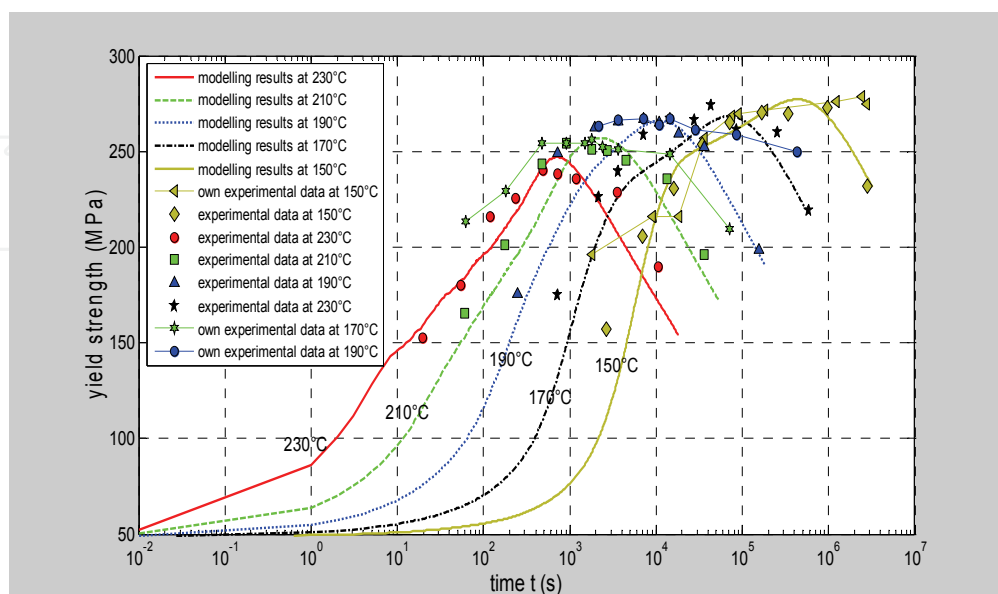


Fig. 5. Modelling results for ageing at various temperatures for A356

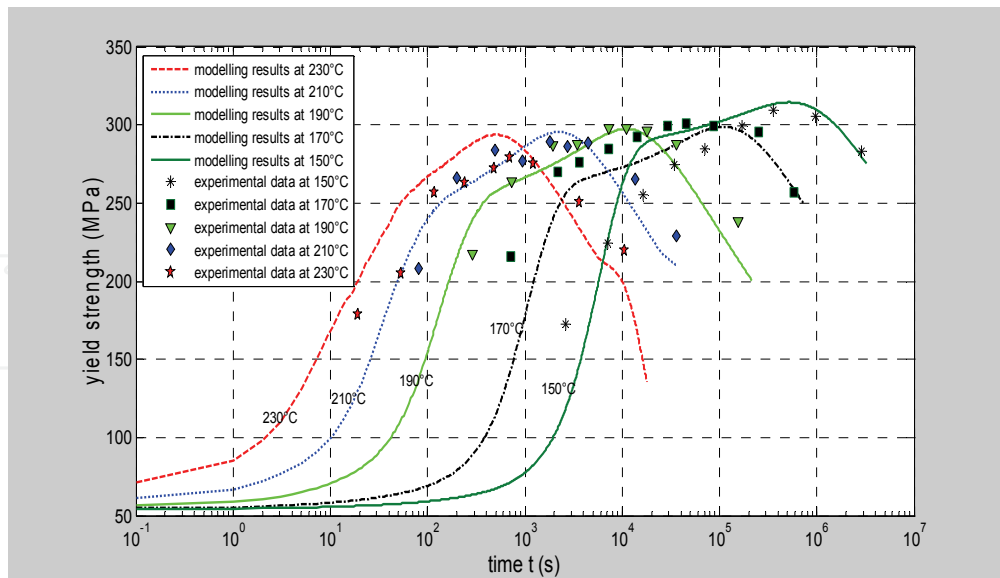


Fig. 6. Modelling results for ageing at various temperatures for A357

Fig. 7 gives the particle size distribution (PSD) after ageing at different temperatures for 3 hours for A356. For this time it is over-ageing for 210°C and 230°C, peak-ageing for 190°C and under-ageing for 170°C. The distribution broadens significantly in going from under ageing to over ageing. The evolution of PSD with time, as shown in Fig.8, indicates the particles gradually move to a larger size and therefore the broadness of the shape of distribution becomes greater with time evolution. Fig. 9 shows how the number of particles per unit volume changes with time at different temperatures.

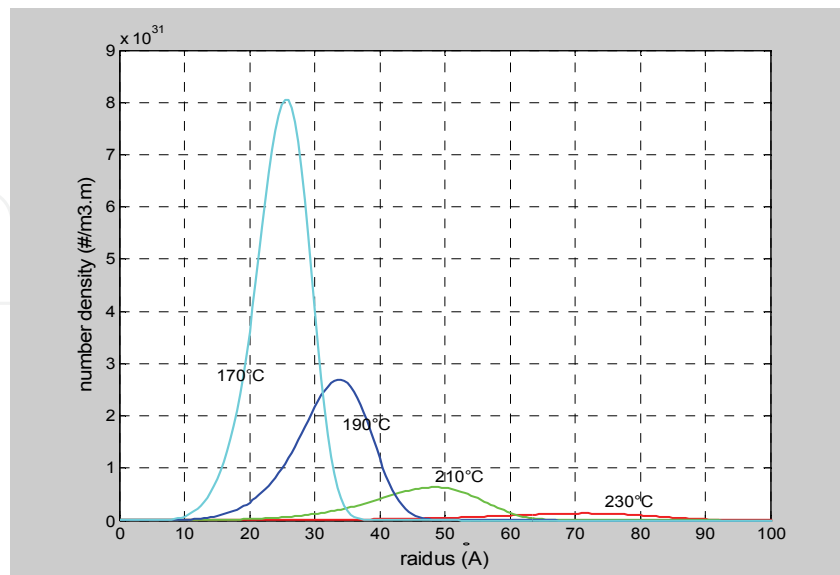


Fig. 7. Particle size distribution (PSD) after ageing: (a) 3 hours for different temperatures for A356

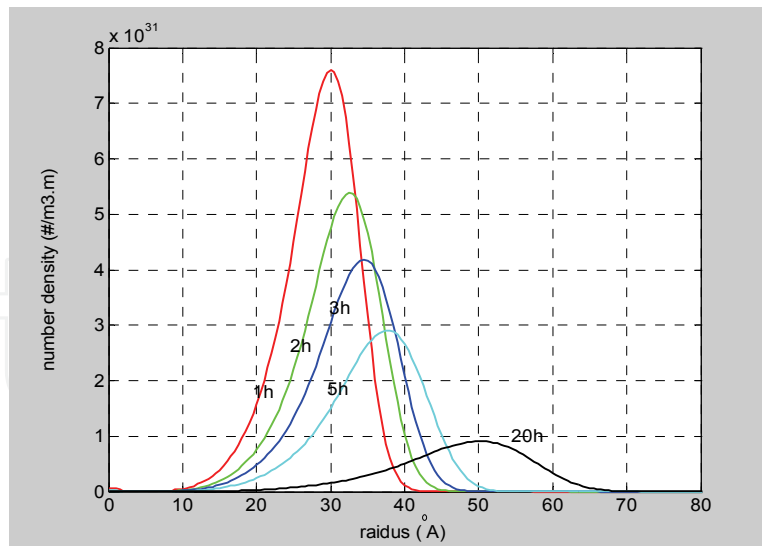


Fig. 8. Particle size distribution (PSD) after ageing different times at 190° C for A357

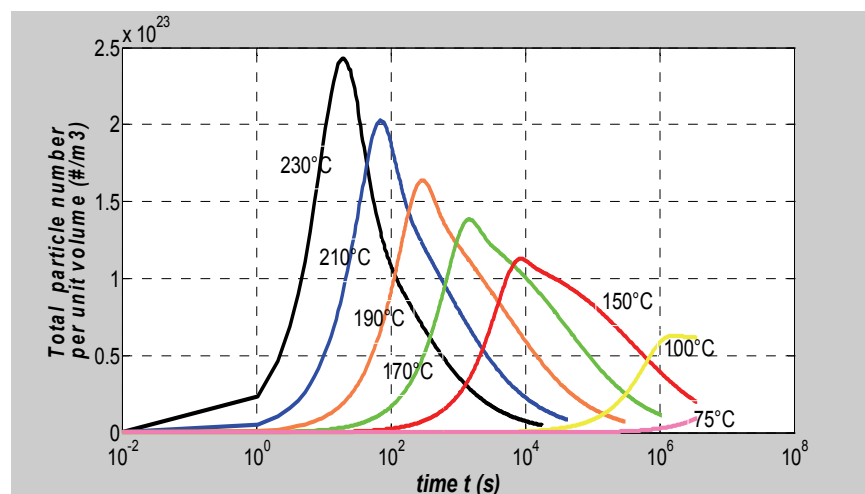


Fig. 9. Evolution of total number of particles per unit volume for ageing at different temperatures for A357

The total number of particles per unit volume increases to the peak value then decreases gradually. For higher temperature, it is faster to the peak value.

4. Comparing with Shercliff-Ashby methodology

Figures Fig.10 and Fig. 11 show the modelling results of yield strength under different ageing temperatures by the Schercliff-Ashby method and the KWN model for A356 and A357 respectively. The key for the figures is: '150-1' stands for modelling at 150°C by method 1- KWN model, '150-2' stands for modelling at 150°C by method 2- Schercliff-Ashby method, and '150-3' stands for experimental data for ageing at 150°C. Other symbols stand for the similar meanings. The experimental data is obtained from Rometsch & Schaffer's work (Rometsch & Schaffer, 2002).

From Fig. 10 and Fig. 11 we can see that most of the experimental data are located between the two modelling methods which means that the results simulated by both methods are in

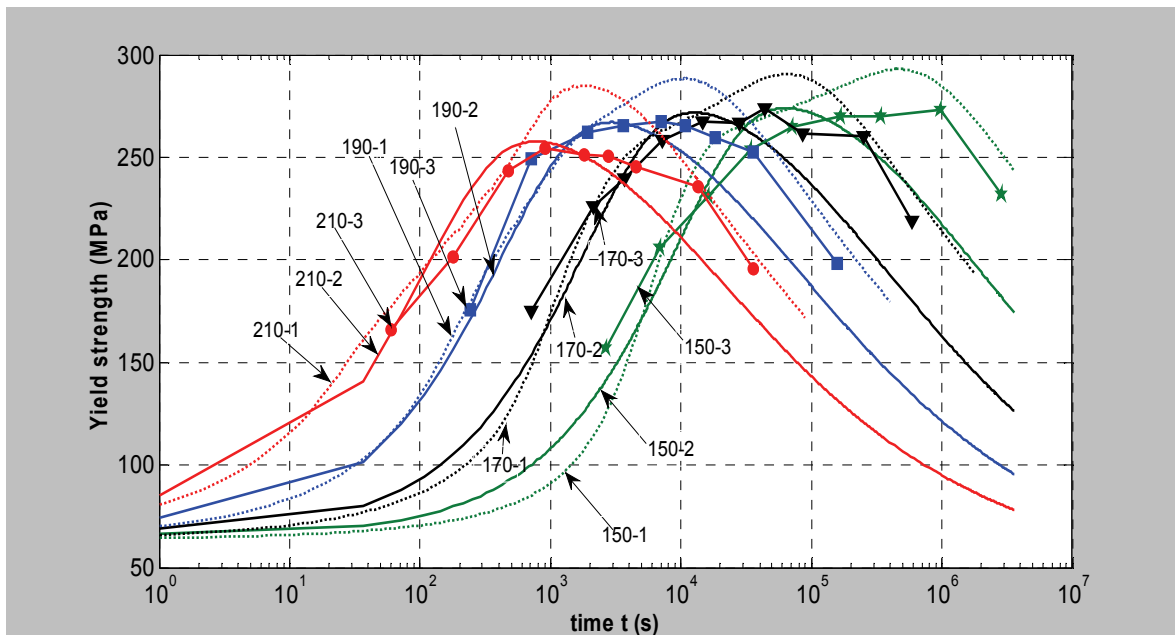


Fig. 10. Modelling of age hardening for A356 at ageing temperatures of 150°C, 170°C, 190°C and 210°C by Schercliff-Ashby method and KWN model, and comparison with experimental data.

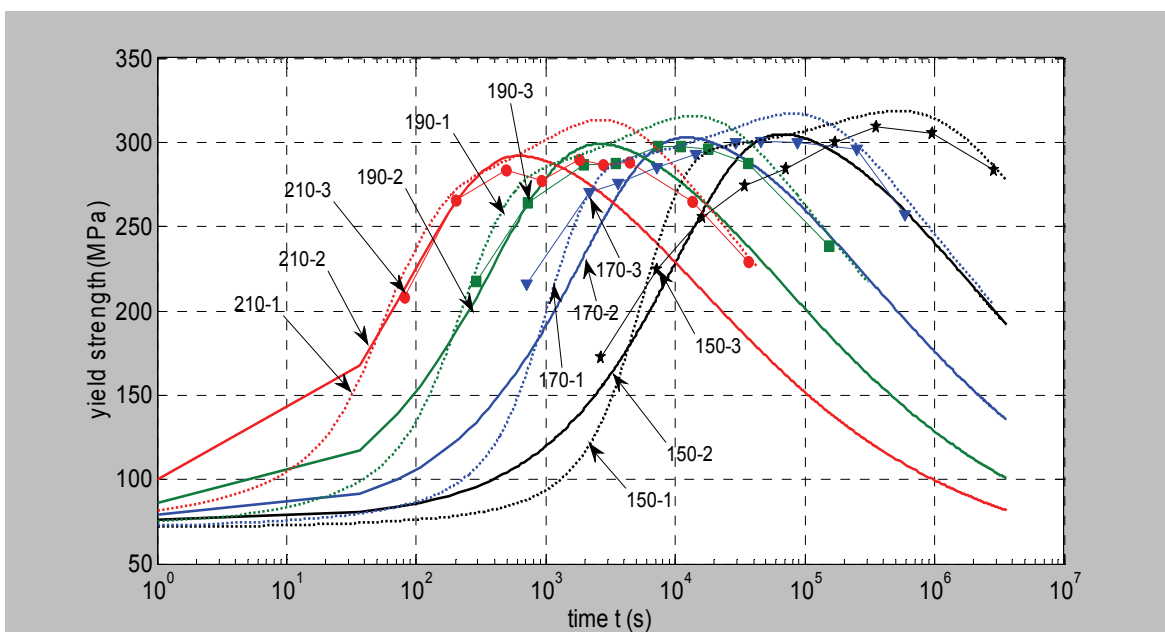


Fig. 11. Modelling of age hardening for A357 at ageing temperatures of 150°C, 170°C, 190°C and 210°C by Schercliff-Ashby method and KWN model, and comparison with experimental data.

reasonable agreement with the experimental data. For the top part of the simulated ageing curve, the broadness is greater with the KWN model than the Schercliff-Ashby method. Therefore, the shape of ageing curves modelled by the KWN model are in closer agreement to the experimental data which means that the KWN model can give a better simulation of results. The reason for this is that the KWN model involves the whole precipitation process that is initiated by nucleation, then proceeds to particle growth and eventually ends with

Ostwald coarsening. These three processes significantly overlap. The existing particles may grow or shrink depending on their size. If the particle size is greater than the critical size, it will grow; otherwise, it will dissolve. Whereas in the Schercliff-Ashby method, the particle size is only controlled by the Ostwald coarsening, no nucleation is considered. However, in the KWN model, not only the time is discretized, but also the continuous size distribution is subdivided into a large number of size classes, which results in a large amount in calculation time. Therefore, the Schercliff-Ashby method is faster than the KWN model. Normally, the Schercliff-Ashby method can be completed in a few minutes, whereas for KWN model, may take about one day to finish the calculation. Moreover, since most constants used in the equations are calibrated from ageing data, the modelled peak yield strength is more accurate for the Schercliff-Ashby method than the KWN model. Furthermore, some constants determined by calibration in the Schercliff-Ashby method, such as activation energy Q_A , solvus enthalpy Q_s , solvus temperature T_s , can also be used in the KWN model. But only when there exist series ageing data, which means series peak yield strength - ageing time to peak yield strength can we use the Schercliff-Ashby method.

5. Conclusions

In the Schercliff-Ashby process model, the most important and difficult part is to calibrate the constants used in the equations from the systematic experimental data (ageing curves). Since lack of information at low temperature for calibration, the modeling results were in poor agreement with the experimental data at low temperatures.

The Kampmann and Wagner numerical (KWN) model can be applied to not only wrought aluminium alloys, but also the casting alloys, such as A356 and A357. By choosing suitable parameters used in the microstructural and strength model, the modelling results are in good agreement with the experimental data obtained from the literature as well as own experimental data. This is the first time that the KWN model has been applied to the casting aluminium alloys.

For the casting aluminium alloys A356 and A357, the modelling results simulated by the KWN model are in better agreement with the experimental data than that by the Schercliff-Ashby method. However, the Schercliff-Ashby method can provide more accurate peak yield strength values and some constants calibrated in the Schercliff-Ashby method can also be used in the KWN model. Therefore, these two modelling methods complement each other.

6. Reference

- Anderson, W.A., (1959) Precipitation from solid solution, ASM, metals park, Ohio
- Ardell, A. (1985) Precipitation hardening. *Metallurgical and Materials Transactions A*, 16, 2131.
- Brown, L.M. & Ham, R.K. (1971) *Dislocation-Particle Interactions, in Strengthening methods in crystals*, eds Kelly, A. and Nicholson, Robin. Amsterdam, New York,: Elsevier Pub. Co.
- Cahn, R.W. & Haasen, P. (1996) *Physical metallurgy*. Elsevier Science Publishers, North-Holland, Amsterdam ; New York.
- Cottrell, A. (1964) *Theory of crystal dislocations*. New York: Gordon and Breach.
- Deschamps, A. & Brechet, Y. (1998) Influence of predeformation and ageing of an Al-Zn-Mg alloy-- II. Modeling of precipitation kinetics and yield stress. *Acta Materialia*, 47, 293.
- Friedel, J. (1964) *Dislocations*, Pergamon Press

- Gerold, V. (1980) Precipitation Hardening, *Dislocations in Solids*, 4, 219.
- Grong, O. (1997) *Metallurgical Modeling of Welding*. The Institute of Materials, London, second ed.
- Hatch, J.E. (1984) *Aluminum : properties and physical metallurgy*. Metals Park, Ohio: American Society for Metals.
- Hospital, J.T. (1987) *Dislocations*. St. Lucia, Qld.: University of Queensland.
- Hull, D. & Bacon, D.J. (2001) *Introduction to dislocations*, 4th edn. Oxford [Oxfordshire] ; Boston: Butterworth-Heinemann.
- Ion, J.C.; Easterling, K.E. & Ashby, M.F. (1984) A second report on diagrams of microstructure and hardness for heat-affected zones in welds. *Acta Metallurgica*, 32, 1949.
- Kampmann, R.; Eckerlebe, H. & Wagner, R., (1987) Precipitation Kinetics in Metastable Solid Solutions-Theoretical Considerations and Application to Cu-Ti Alloys. In: *Phase Transitions in Condensed Systems--Experiments and Theory*: 525. Boston, Massachusetts; USA; .
- Kampmann, R. & Wagner, R., (1984) Kinetics of Precipitation in Metastable Binary Alloys-Theory and Application to Cu-1.9at% Ti and Ni-14at% Al. 91.
- Kocks, U.F.; Argon, A.S. & Ashby, M.F. (1975) Thermodynamics and Kinetics of Slip. *Progress in Materials Science*, 19, 1.
- Langer, J.S. & Schwartz, A.J. (1980) Kinetics of nucleation in near-critical fluids. *Physical Review A*, 21, 948.
- Lifshitz, I.M. & Slyozov, V.V. (1961) The kinetics of precipitation from supersaturated solid solutions. *Journal of Physics and Chemistry of Solids*, 19, 35.
- Lloyd, D.J. (1985) Precipitation Hardening. *Strength of Metals and Alloys (ICSMA 7)*, 3, 1745.
- Madras, G. & McCoy, B.J. (2003) Temperature effects for crystal growth: a distribution kinetics approach. *Acta Materialia*, 51, 2031.
- Martin, J.W. (1980) *Micromechanisms in particle-hardened alloys*. Cambridge ; New York: Cambridge University Press.
- Miyazaki, T.; Koyama, T. & Kobayashi, S. (1996) A new characterization method of the microstructure using the macroscopic composition gradient in alloys. *Metallurgical and Materials Transactions A*, 27, 945.
- Myhr, O.R. & Grong, O. (2000) Modelling of non-isothermal transformations in alloys containing a particle distribution. *Acta Materialia*, 48, 1605.
- Myhr, O.R.; Grong, O. & Andersen, S.J. (2001) Modelling of the age hardening behaviour of Al-Mg-Si alloys. *Acta Materialia*, 49, 65.
- Myhr, O.R.; Grong, Ø.; Fjær, H.G. & Marioara, C.D. (2004) Modelling of the microstructure and strength evolution in Al-Mg-Si alloys during multistage thermal processing. *Acta Materialia*, 52, 4997.
- Myhr, O.R.; Grong, Ø.; Klokkehaug, S. & Fjær, H.G., (2002) Mathematical Modelling of Weld Phenomena. Bhadeshia, H.K.D.H. (Ed.). London: Maney Publishing.
- Myhr, O.R.; Klucken, A.O.; Klokkehaug, S.; Fjaer, H.G. & Grong, O. (1998) Modeling of microstructure evolution, residual stresses and distortions in 6082-T6 aluminum weldments. *Welding Journal ; VOL. 77 ; ISSUE: 7 ; PBD: Jul 1998*, pp. 286.s.
- Nabarro, F.R.N. (1967) *Theory of crystal dislocations*. Oxford,: Clarendon P.
- Nabarro, F.R.N.; Duesbery, M.S. & Hirth, J.P. (1979) *Dislocations in solids*. Amsterdam ; New York: North-Holland Pub. Co.

- Orowan, E. (1948) *Symposium on Internal Stresses in Metals and Alloys, Session III discussion*.
- Ostwald, W. (1900) Über die Vermeintliche Isomerie des Roten und Gelben Quecksilberoxyds und die Oberflächenspannung Fester Körper. *Z. Phys. Chem.*, 34, 495.
- Pandey, A.D., (1995) A process model for age-hardening in aluminum-lithium alloy AA8090. The University of Regina (Canada), Canada.
- Polmear, I.J. (2006) *Light alloys : from traditional alloys to nanocrystals*, 4th edn. Amsterdam ; London : Elsevier Butterworth-Heinemann.
- Porter, D.A. & Easterling, K.E. (1992) *Phase transformations in metals and alloys*, 2nd edn. London ; New York: Chapman & Hall.
- Robson, J.D. (2004a) Microstructural evolution in aluminium alloy 7050 during processing. *Materials Science and Engineering A*, 382, 112.
- Robson, J.D. (2004b) Modelling the overlap of nucleation, growth and coarsening during precipitation. *Acta Materialia*, 52, 4669.
- Robson, J.D. (2008) Modelling precipitation in zirconium niobium alloys. *Journal of Nuclear Materials*, 377, 415.
- Robson, J.D.; Jones, M.J. & Prangnell, P.B. (2003) Extension of the N-model to predict competing homogeneous and heterogeneous precipitation in Al-Sc alloys. *Acta Materialia*, 51, 1453.
- Rometsch, P.A. & Schaffer, G.B. (2002) An age hardening model for Al-7Si-Mg casting alloys. *Materials Science and Engineering A*, 325, 424.
- Sanders, T.H., 1980, *Stone Mountain, Ga*.
- Shercliff, H.R. & Ashby, M.F. (1990a) A process model for age hardening of aluminium alloys--I. The model. *Acta Metallurgica et Materialia*, 38, 1789.
- Shercliff, H.R. & Ashby, M.F. (1990b) A process model for age hardening of aluminium alloys--II. Applications of the model. *Acta Metallurgica et Materialia*, 38, 1803.
- Shewmon, P.G. (1963) *Diffusion in solids*. New York,: McGraw-Hill.
- Starke, E.A. (1977) Aluminium alloys of the 70's: Scientific solutions to engineering problems. An invited review. *Materials Science and Engineering*, 29, 99.
- Swalin, R.A., (1962) *Thermodynamics of Solids*. Wiley, New York
- Wagner, C. (1961) Theorie der alterung von niederschlägen durch unlösen. *Z. Elektrochem*, 65, 581.
- Wagner, R.; Kampmann, R. & Voorhees, P.W., (1991) Homogeneous second-phase precipitation. In: *Materials science and technology : a comprehensive treatment*. Cahn, R.W.; Haasen, P. & Kramer, E.J. (Eds.). Wiley-VCH, Weinheim.
- Wilm, A. (1911) Physikalisch-metallurgische untersuchungen über magnesiumhaltige aluminiumlegierungen. *Metallurgie*, 8, 225.



Aluminium Alloys, Theory and Applications

Edited by Prof. Tibor Kvackaj

ISBN 978-953-307-244-9

Hard cover, 400 pages

Publisher InTech

Published online 04, February, 2011

Published in print edition February, 2011

The present book enhances in detail the scope and objective of various developmental activities of the aluminium alloys. A lot of research on aluminium alloys has been performed. Currently, the research efforts are connected to the relatively new methods and processes. We hope that people new to the aluminium alloys investigation will find this book to be of assistance for the industry and university fields enabling them to keep up-to-date with the latest developments in aluminium alloys research.

How to reference

In order to correctly reference this scholarly work, feel free to copy and paste the following:

Linda Wu and W. George Ferguson (2011). Modelling of Precipitation Hardening in Casting Aluminium Alloys, Aluminium Alloys, Theory and Applications, Prof. Tibor Kvackaj (Ed.), ISBN: 978-953-307-244-9, InTech, Available from: <http://www.intechopen.com/books/aluminium-alloys-theory-and-applications/modelling-of-precipitation-hardening-in-casting-aluminium-alloys>

INTECH
open science | open minds

InTech Europe

University Campus STeP Ri
Slavka Krautzeka 83/A
51000 Rijeka, Croatia
Phone: +385 (51) 770 447
Fax: +385 (51) 686 166
www.intechopen.com

InTech China

Unit 405, Office Block, Hotel Equatorial Shanghai
No.65, Yan An Road (West), Shanghai, 200040, China
中国上海市延安西路65号上海国际贵都大饭店办公楼405单元
Phone: +86-21-62489820
Fax: +86-21-62489821

© 2011 The Author(s). Licensee IntechOpen. This chapter is distributed under the terms of the [Creative Commons Attribution-NonCommercial-ShareAlike-3.0 License](#), which permits use, distribution and reproduction for non-commercial purposes, provided the original is properly cited and derivative works building on this content are distributed under the same license.

IntechOpen

IntechOpen